A Multi-Layer Framework for Reliability Assessment of Shore-to-Ship Fast Charging System Design

Siamak Karimi, *Student Member, IEEE*, Mehdi Zadeh, *Member, IEEE* and Jon Are Suul, *Member, IEEE*

[1]***Abstract*— In this paper, a multi-layer framework is proposed to assess the reliability of Shore-to-Ship Charging (S2SC) systems, considering the potential for failures of the main elements, such as power converters and batteries. The proposed reliability model enables evaluating a S2SC system with redundancy, multi-state system availability, and multi-variable design scenarios, based on a recursive algorithm. Instead of conventional Markov-chain multi-state models, a reduced order state-space model is established from a set of specific sub-systems with a predefined configuration complying with the design requirements. A modular approach is taken, and the probabilistic characteristics of the sub-systems are established by developing a Universal Generating Function considering the available charging power and energy balance constraints. Then, the sub-systems are integrated into the system configuration to assess a set of proposed application-specific system-level reliability indices. Thus, the modular approach enables expansion to the power system dimensions without extra complexity. Finally, a case study based on an operating 4-MW dc S2SC system is performed by the proposed framework, and design suggestions are given based on a figure of merit defined for evaluation of reliability and energy efficiency. These design suggestions include resizing the charging system by installing onshore batteries, modularization, and introduction of redundancy in the sub-systems.**

***Index Terms*— all-electric ships, marine electrification, multi-state systems, redundancy, reliability analysis, shore-to-ship charging, universal generating function.**

I. Introduction

Shore-to-ship charging (S2SC) bridges the marine transportation to the land-based power system which can be fed by a mix of sustainable energy sources, such as wind, solar power, and hydropower etc., in addition to traditional fossil fuel-based power plants [1]. The battery-powered and plug-in hybrid vessels with electric propulsion can then receive charging from shore during the docking period while loading and unloading. Such S2SC systems are under development for a wide range of electrified (and autonomous) vessels, mainly ferries, regional freight transportation and cruise vessels, which typically operate with a preplanned schedule [2]. Therefore, the charging process is constrained within a critical time, often in the order of a few minutes for short-distance ferries. If a fault hindering the charging process happens in the S2SC system, it causes inconvenience for the vessel passengers and expensive fines for the ship operators due to cancellations or delayed schedules [3]. In this regard, the reliability and availability of the S2SC system is a crucial design factor considering the significant cost of system outages.

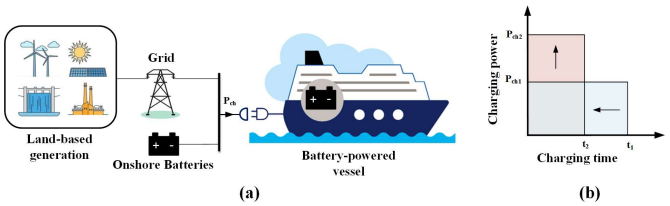

Fig. 1. (a) a S2SC system with onshore batteries (b) the charging power vs charging time for a constant charging energy.

When vessels depending on S2SC are operating in remote locations with a weak distribution grid – e.g., in Norwegian fjords – additional stationary onshore batteries, i.e., On-Shore Battery (OSB) storage systems, are used to support the grid in supplying the high-power demand as indicated in Fig. 1. (a) a S2SC system with onshore batteries (b) the charging power vs charging time for a constant charging energy.

(a). Therefore, a practical S2SC system in its general form includes three sub-systems, i.e., OSB, a Grid Interface (GI) and the On-Board Battery (OBB) energy storage system as the receiver of the charging energy [1]. The unavailability or outage of the S2SC systems can occur due to outages of the distribution grid – as the energy source for the charging operations – or failures in the charging system, including in the GI, OSB and OBB subsystems [4]. In a S2SC system for vessels with tight schedules, the power and energy requirements are normally high, in the order of several MWs, due to the critical charging time and large onboard batteries required for the fully electric operation. As it is shown in Fig. 1. (a) a S2SC system with onshore batteries (b) the charging power vs charging time for a constant charging energy.

Manuscript received April 1, 2021; revised June 28, 2021; accepted August 1, 2021. Date of publication x, x; date of current version x, x. This work was supported by Center for research-based innovation smart maritime, Norway. (Corresponding author: Mehdi Zadeh.)

S. Karimi and M. Zadeh with the Department of Marine Technology, Norwegian University of Science and Technology (NTNU), 7052 Trondheim, Norway (e-mail: siamak.karimi@ntnu.no; mehdi.zadeh@ntnu.no).

J. A. Suul is with SINTEF Energy Research, also with the Department of Engineering Cybernetics, Norwegian University of Science and Technology (NTNU), Norway (e-mail: jon.a.suul@sintef.no).

(b), transferring a specified charging energy during a reduced charging time, due to a tighter schedule, would increase the charging power requirement.

Although the reliability and lifetime evaluation of power electronics converters have been the topic of extensive research in recent years [5], no organized system-level approach has been established for the evaluation of reliability and availability of marine power systems. Thus, research on the system-level reliability of the onboard power systems and charging systems for the transportation electrification is still developing. The previous research on related topics ranges from the reliability assessment of the onboard power system of the more-electric aircrafts [6], [7], the shipboard power system [8], [9] and the electric vehicles [10] to the reliability of PV systems [11]. In such studies, well-known reliability methods are employed to assess the system in terms of faulty-healthy states or the standard adequacy indices defined for power systems [12]. Instead, specific reliability indices for S2SC systems are introduced in this work.

To improve the reliability, redundancy-based design has been suggested in the literature, for instance applied to phases of an interleaved boost converter [13], arms in a modular multilevel converter [14] and paralleled inverters in a distribution system [15]. Nevertheless, the impact of the redundancy of the components in different sub-systems in a holistic manner, as opposed to one specific component through a load-dependent reliability analysis, has not been studied in such research papers.

There have been only few studies addressing the reliability of shore connection systems [16], [17]. In [17], a reliability block diagram has been proposed for the shore to ship connection. Nevertheless, it considered only the cold-ironing and not the shore charging. One of the common methods to assess the reliability of a multi-state system is the Markov chain, in which all the possible states with the transition rates between them are studied to derive the reliability indices of the system. Such an approach was carried out for two S2SC topologies in [16] by establishing the Markov chain of the whole system. However, in that method, any slight change in the configuration of the system will require the modification of the state space model. On the other hand, by such a Markov-chain approach, the state space model will grow exponentially with the increase in the number of the components. Other than Markov chain, Fault tree analysis [18], capacity outage probability table [19] and Universal Generating Function (UGF) [20] approaches were employed to predict the reliability of multi-state systems.

The reliability-critical components of the S2SC systems are the Li-ion batteries – both onshore batteries and onboard batteries – and the associated power electronic converters. Regarding the reliability analysis of the Li-ion batteries, there has been several studies in the literature related to the stationary batteries as well as electric vehicles; some of which used statistical methods based on the lifetime of the batteries [21], [22] while others used the constant failure rate for the batteries based on the block diagram method considering different components of a battery storage system [23], [6]. For the power electronics converters, only the semiconductor devices and capacitors are usually considered as the reliability-critical parts [5]. For the reliability analysis of such elements, the two main approaches used in practice are the lifetime model-based reliability [11] and the reliability prediction based on historical data [22]. The lifetime models relying on physics-of-failure-based analysis can account for the aging effect of components based on the thermal cycling and lifetime models [11]. However, this approach suffers from the high computational effort. The historical-data-based models are usually established based on the data available in the reliability handbooks [18] and avoids the complexity of the lifetime models at the expense of lower accuracy. The historical reliability models obtain the failure rate of the parts for the certain operation conditions. In the power electronics systems, the operating conditions include the voltage stress, the power loading, and the junction temperature rise due to the power dissipation in the power converters [22].

In a high power S2SC system, the sub-systems are usually constructed from modules connected in parallel, to reach the required power levels but also to enhance the reliability and resilience of the system. The charging busbar is also usually designed such that it can be split into two or more sections by bus-tie breakers [24]. In this case, the failure of a single component may not end in the final failure of the system. Rather, the charging mission might be continued at a lower charging power in the derated states, resulting in a multi-state system model in terms of operation and reliability/availability.

Given the above-mentioned facts, there are major differences between land-based power electronics systems and the S2SC systems. Indeed, the reliability and availability of S2SC systems is “ship profile-based,” necessitating the following considerations:

1) In a S2SC system, the mission is to charge the onboard batteries with a certain energy (and by the nominal charging power) within a specified time. Thus, if a certain set of component failures occur, the S2SC system may not be able to provide the nominal charging power requested by the vessel. Consequently, the vessel may continue its operation within the predefined schedule only if the remaining energy in the OBB after the compromised charging process is sufficient for the next trips. Hence, instead of a conventional reliability analysis by considering the states of the system as failed/healthy, application-specific thresholds, constrains and reliability indices are to be defined.
2) On contrary to the systems with multiple sources, the S2SC systems usually relies on the GI and an energy buffer which is the OSB. Then, firstly, the performance of the system is dependant on the availability of the GI and the energy balance of the OSB. Secondly, if the OSB is only designed to avoid overload on the grid, or if the grid is not highly stressed especially in off-peak hours, a failure of the OSB can be compensated by the GI to provide the nominal charging power. Hence, the failure modes are to be defined based on the mission profile of each sub-system that can be also variable.
3) The inherent modularity and redundancy in the design of system elements increases the order of the system model which implies the need for modular techniques for the reliability assessment rather than conventional models.

Moreover, as the design space with feasible design scenarios grows, an automated design routine can help with several aspects, such as minimizing human error and improving functionality. In this work, a comprehensive multi-layer framework containing a recursive algorithm is proposed for the reliability assessment of S2SC systems. Such automated algorithm enables benchmarking the design scenarios in the preliminary system design phase. The proposed approach evaluates the reliability of the system in 4 layers: 1) parts, 2) components, 3) sub-systems and 4) the entire system. In the part level, a constant failure rate of the battery cells and power electronics devices are estimated based on the operational profile and the design parameters of the S2SC system. Then, the reliability of the components is calculated based on the calculated failure rates of the parts. In the next layer, the state-space diagram of the sub-systems, which are composed of several components, are established by Markov chain approach with the state-dependant failure rates to account for the redundancy. In other words, the loading of components depends on the redundancy of the system, and consequently the estimated failure rates are affected. Unlike the conventional Markov-based methods for the whole system, which may lead to state explosion, the proposed state-space model has a predefined configuration, for example, a sub-system with *n* identical components in parallel. As a result, the probability calculation would not be affected by the increase in the number of the units. Moreover, in cases with more than one bus-section in the system, the probability of the whole sub-system is obtained by a composition operator through the UGF approach. It is worth mentioning that such predefined structures within the sub-systems enables the assessment of the system independently from the number of the components. Nonetheless, justifying the modified topologies of the sub-systems, the framework has the potential to be updated by only modifying the Markov chains in the sub-system layer. In the final layer of the algorithm, the probability tables of the GI and OSB sub-systems are integrated by a defined composition operator through the UGF, considering the constraint for energy balance of the OSB. Then, the OBB probability table and the GI-OSB probability table are composed by mean of a defined composition operator. Finally, the application-specific indices and constrains which are suggested and formulated to capture the performance of the S2SC system are calculated.

The results of such practical and rather informative reliability assessment can be utilized to assess the required redundancy and estimated system availability. As a result, a partial preliminary design tool including the suggestion of parts/components and sizing of components/sub-systems to achieve higher reliability can be introduced. In the proposed method, the redundancy can also be assigned to each component/sub-system based on its impact on the total system performance, as a so called, distributed redundancy.

To apply the proposed framework on a practical S2SC system, a case study is caried out based on the field data of the 4-MW charging system for the E-ferry Ellen [25]. In order to provide a practical evaluation for the system design, a Figure of merit (FoM) is established including the reliability indices and the estimated energy efficiency. Here, the assessment of the energy efficiency is based on the model presented in [4]. Then, different design scenarios are evaluated based on the suggested FoM, and design candidates are introduced consequently. Finally, for a design candidate, the effect of distributed redundancy in the sub-system design on the reliability indices, energy efficiency and the FoM is investigated.

The rest of this paper is structured as follows. The S2SC system realization and the introduction of the reliability indices are given in section II. Section III is dedicated to the proposed reliability analysis method in which the recursive approach is explained step by step. Finally, the case study and the results are presented and discussed in the section IV.

II. Configuration and Characterization of the Shore-to-ship Charging System

The dc S2SC system considered for this study is shown in Fig. 2. In this configuration, the onboard transformers and rectifiers needed for ac charging can be avoided since the charging connection is by direct current. The grid is interfaced by one transformer per section and N_{GI} active rectifiers connected in parallel. Further, the onshore battery systems, which are sectioned into two rooms, are constituted by N_{OSB} battery units including a battery pack and its dedicated dc-dc converter. Similarly, the onboard batteries are divided into two rooms, in each of which there are N_{OBB} battery units. Similar solutions have been developed for charging E-ferry Ellen with 780Vdc [25] and MF Future of The Fjords with 1000Vdc [26].

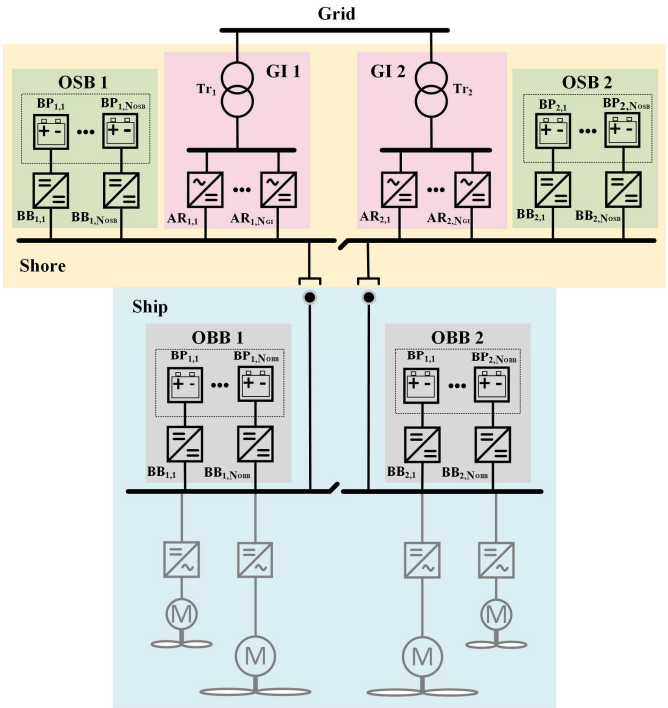

Fig. 2. The single line diagram of an all-electric ship with dc shore-to-ship charging ($BB_{i,j}$: the j^{th} Buck/Boost converter in i^{th} bus section, $AR_{i,j}$: the j^{th} Active Rectifier in i^{th} bus section and $BP_{i,j}$: the j^{th} Battery Pack in i^{th} bus section.)

In a S2SC system, the amount of the required charging power at each charging break is calculated online in the onboard power management system based on the operational factors [1]. However, the planned charging profile can be used for design

purposes. Due to the modularity of the system from Fig. 2, the failure of one or a set of components may not lead to the final failure of the system. Thus, in the following, a threshold to specify the derated operation states is defined. In the normal operation of a battery-powered passenger/car ferry, the onboard battery is discharged to supply propulsion loads during operation within trip time, t_{tr}, and recharged with charging power, P_{ch}, at docking within charging time, t_{ch}. For simplicity, it is assumed that the discharged and charged energy of the onboard batteries remain constant in all the n trips. The energy equilibrium for the onboard batteries can be written as follows.

$$\sum_{i=1}^{n-1}\left(P_{ch,i}t_{ch,i}\right)-\sum_{i=1}^{n}E_{tr,i}=(SoC_F-SoC_I)C_s \qquad (1)$$

in which E_{tr} and C_s are the discharged energy from the onboard batteries during the trips and the capacity of the onboard batteries. SoC_I and SoC_F are the initial and final value of equivalent SoC of the onboard batteries during one day of operation. Because of the safety and lifetime of the batteries, the SoC of the batteries should remain with the SoC_{Max} and SoC_{Min} which can be defined as 90% and 15%, for example [25]. However, considering the optimum lifetime of the batteries, the operational parameters are usually designed in such a way that the SoC range within the operation do not reach the maximum and minimum values. Rather, the state of the charge of the onboard batteries starts at SoC_U at the beginning of the trip and end up in SoC_L at the end of a trip.

$$SoC_{Min}\le SoC_L<SoC_U\le SoC_{Max} \qquad (2)$$

Given the trip and docking times as well as propulsion power being constant during one day of operation, the final SoC at the end of the day can vary depending on the charging power as shown in Fig. 3.

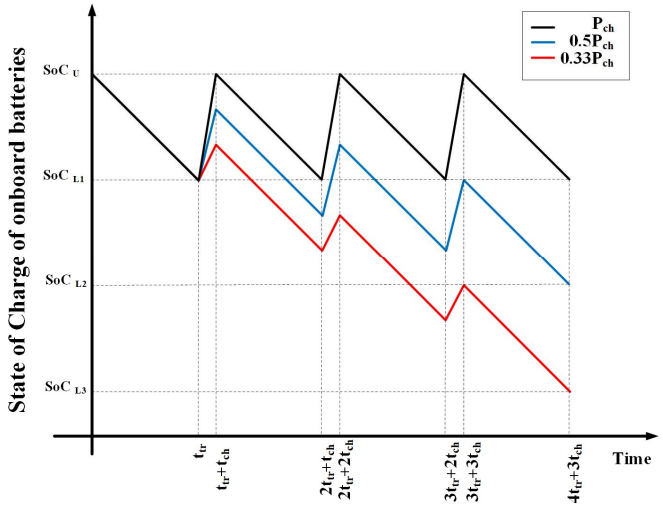

Fig. 3. An example of the energy profile of onboard batteries

In case of reduced charging power, the ferry can continue operating as far as the onboard battery SoC does not reach the minimum safety value. Therefore, the failure threshold can be defined as the minimum charging power by which the ferry can continue operation until the failed submodules are repaired. In this regard, it is assumed that the failure happens before the first charging interval and the charging mission should be carried out for one full day of operation without any impact on the ferry schedule. This charging power threshold can be calculated by equation (3), considering the final SoC, SoC_F, to be equal to SoC_{Min} in (1).

$$P_{ch}^{Th}=\frac{(SoC_{Min}-SoC_I)C_s+nE_{tr}}{(n-1)t_{ch}} \qquad (3)$$

Hence, the operation states are categorized into three classes; 1) normal operation with the nominal charging power, 2) derated operation with charging power more than the threshold and lower than the nominal value for which the minor maintenance can revive the system and 3) final failure operation with charging power less than the threshold and with major maintenance required. Inspired by the probabilistic indices used for the power system, such as Loss of Load Expectation (LOLE) in which the probability of not being able to supply the forecasted peak load within a year is calculated [5], three application-specific indices are defined for S2SC. The first one is Loss of Charging Expected (LOCE) indicated the number of failed charging breaks per year and it is obtained as follows:

$$\begin{aligned}LOCE&=\sum_{i=1}^{365}\sum_{j=1}^{n}\Pr\left(P_{ch}<P_{ch}^{Th}\right)\\&=365\sum_{j=1}^{n}\Pr\left(P_{ch}<P_{ch}^{Th}\right)\end{aligned} \qquad (4)$$

where $Pr(.)$ is the probability of charging operation associated with the charging power P_{ch} and is calculated by the reliability analysis. The second index which is called Derated Charging Expected (DCE) indicated the number of charging breaks per year when that the charging has been compromised due to the faults.

$$\begin{aligned}DCE&=\sum_{i=1}^{365}\sum_{j=1}^{n}\Pr\left(P_{ch}^{Th}<P_{ch}<P_{req-i,j}\right)\\&=365\sum_{j=1}^{n}\Pr\left(P_{ch}^{Th}<P_{ch}<P_{req-i}\right)\end{aligned} \qquad (5)$$

in which $P_{req-i,j}$ is the required charging power at the i^{th} day of the year in the j^{th} charging break. Additionally, the Available Charging Power (ACP) index would represent the averaged capability of the system statistically, and as the available charging power increases the availability of the system would improve. This index is calculated as following in which m is the number of operation states in the probabilistic characteristic of the system.

$$ACP=\sum_{i=1}^{m}\Pr\left(P_{ch,i}\right).P_{ch,i} \qquad (6)$$

III. Reliability Assessment Framework

First, in terms of its performance and the compatibility with the main characteristics of S2SC systems, the proposed framework is compared with the common reliability analysis approaches in Table I. Note that the comparison relies on the assumption that the reliability assessment is based solely on each method in its basic form.

TABLE I
Comparison Between the Proposed Framework and the Conventional Reliability Analysis Approaches for S2SC Systems

Reliability analysis approach	Reliability Block Diagram [18]	Markov chain [16]	Capacity outage probability table [19]	The proposed framework
Compatibility to multi-state model	no	yes	yes	yes
Dependence on system order	high	high	moderate	moderate
Design of redundancy	none	manually	manually	automatically
Computational effort	low	high	moderate	moderate

As it can be seen from the comparison given in TABLE I, the proposed framework outperforms the other conventional methods by enabling the design methods with component sizing and redundancy allocation. In the following, the reliability assessment method is presented step by step, as demonstrated in the flowchart in

. Here, the reliability calculation starts from the lowest to the highest level of hierarchy in the system which is assumed to be parts, such as power electronics elements and battery cells; Components, namely, the converters and battery packs; sub-systems which are OSB, GI and OBB and in the end the whole S2SC system. However, before the reliability assessment begins, the configuration of the system is designed in the S2SCS design stage based on the required charging power, capacity of the sub-systems and the capacity of the components. In addition to the choice of the parts, the redundancy design which is defined as the number of parallel units in the sub-systems are carried out in the design level. Further, after the calculation of the reliability through the four steps, the reliability indices introduced in the section II are calculated and compared with the requirements. Consequently, the redundancy of the system should be improved if the reliability indices are not satisfactory, and the assessment steps would be redone.

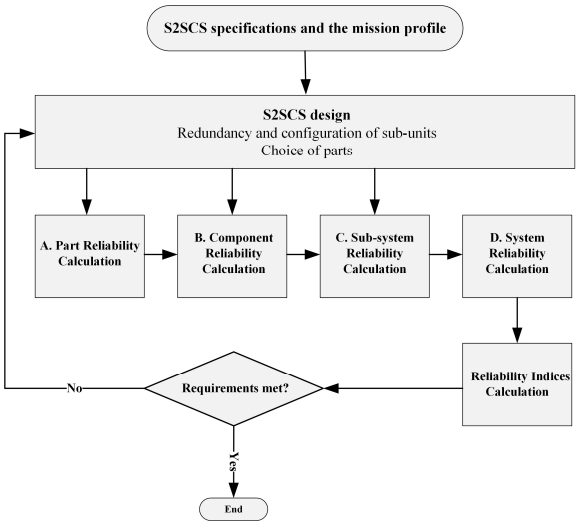

Fig. 4. Proposed reliability-assessment framework for S2SC system.

A. Part reliability calculation

The parts in a S2SC system are the Li-ion battery cells, transformers and the power electronics elements including IGBT, diode and capacitor. The choice of parts from different manufacturer or different ratings can affect the calculated reliability of the whole system. The failure rates of the power electronics parts are extracted from MIL-HDBK-217F in terms of the influencing factor, namely, temperature, voltage ratio and power. However, the other coefficients including environment and quality factors are assumed to be constant [27].

TABLE II
Failure Rates of Parts in Failure/10^6hour [28], [27], [23]

Parts	Failure rate
IGBT	$\lambda_{IGBT} = 0.003 \exp\left(-2114\left(\frac{1}{T}-\frac{1}{298}\right)+3.1V_{st}\right).P^{0.37}$
Diode	$\lambda_{IGBT} = 0.003 \exp\left(-3091\left(\frac{1}{T}-\frac{1}{298}\right)\right).V_{st}^{2.43}$
Capacitor	$\lambda_{Cap} = 0.12 \exp\left(-1.82\times10^{-8}\left(\frac{1}{T}-\frac{1}{298}\right)\right).\left(1+\left(\frac{V_{st}}{0.6}\right)^5\right).C^{0.23}$
Transformer (Liquid filled)	$\lambda_{Trans} = 0.243w$
Li-ion battery cell	$\lambda_c = \lambda_c(1.5)^{\frac{\Delta T}{10}}$

In Table II, T, P and V_{st} are the temperature in K, the power rating in W and the ratio of the break-out voltage over the rated voltage. Further, C, w and ΔT are the capacitance in F, the number of the windings and the battery cell temperature rise.

B. Component reliability calculation

From the reliability point of view, in this work, components are assumed to be made of a set of parts introduced in the previous sub-section.

1) Battery pack: the hierarchy of batteries usually ranges from battery cells, battery modules, battery packs and battery rooms as it is shown in the Fig. 5 In this work, the battery modules are assumed to be made of a parallel connection of p strings including s cells in series. Then, the battery packs consist of q battery modules connected in series and are interfaced by a dedicated bidirectional dc/dc converter. To obtain the reliability of a battery pack as a unit based on the failure rate of a single cell, λ_C, and the configuration of the battery packs, the following expression is used to calculate the failure rate of a battery pack, λ_{BP} [29].

$$\lambda_{BP} = q\left(\frac{s.\lambda_C}{\sum_{i=p_1}^{p}\frac{1}{i}}\right) \tag{7}$$

In which p_1 is the maximum number of the parallel strings in a module which is required to be working. Regarding the temperature rise calculation, which is essential for estimating the failure rates, the power loss generated in one cell based on the battery pack charging/discharging

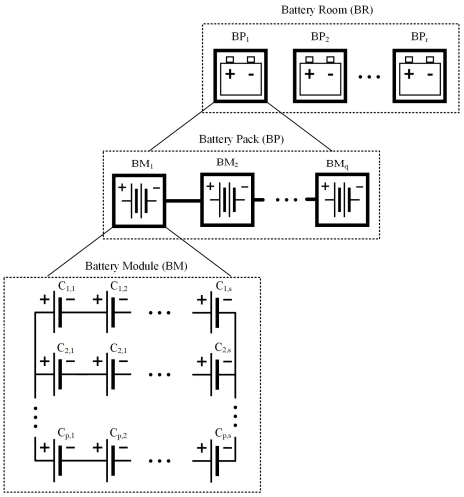

Fig. 5. Configuration of a battery pack and battery module.

power is calculated in (8) [23]. Note that v is the battery cell voltage.

$$P_{loss-cell} = r_i\left(\frac{I_{BP}}{p}\right)^2 = r_i\left(\frac{P_{BP}}{p(s.q.v)}\right)^2 \quad (8)$$

2) Power electronics converters: The failure rate of the power converters used in a S2SC system which are made of a set of critical power electronics parts, i.e., IGBTs, diodes and capacitors, are listed in Table III. Moreover, in order to calculate the temperature rise required to estimate the failure rates in Table II, the power loss models are listed for each specific component in the following table.

TABLE III
POWER CONVERTER UNIT FAILURE RATE [4]

Component	Part	Power loss	Component failure rate
dc/ac converter (AR)	IGBT	$\left(\frac{1}{2\pi}+\frac{m}{8}\right)V_{CE0}\frac{P}{\sqrt{3}V_{ac}} + \left(\frac{1}{8}+\frac{m}{3\pi}\right)r_{CE}\left(\frac{P}{\sqrt{3}V_{ac}}\right)^2 + \frac{\sqrt{2}f_{sw}(E_{sw})}{\pi}\frac{P}{\sqrt{3}V_{ac}I_{ref}}\left(\frac{V_{ce}}{V_{ref}}\right)^{1.3}$	$6(\lambda_{IGBT} + \lambda_{Diode}) + n_{c1}\lambda_{Cap}$
	Diode	$\left(\frac{1}{2\pi}-\frac{m}{8}\right)V_{FW0}\frac{P}{\sqrt{3}V_{ac}} + \left(\frac{1}{8}-\frac{m}{3\pi}\right)r_F\left(\frac{P}{\sqrt{3}V_{ac}}\right)^2 + \frac{\sqrt{2}f_{sw}(E_{rr})}{\pi}\left(\frac{P}{\sqrt{3}V_{ac}I_{ref}}\frac{V_{ce}}{V_{ref}}\right)^{0.6}$	
	Capacitor	$\frac{\tan\delta}{2\pi f_{sw}C}(I_h)^2$	
dc/dc converter (BB)	IGBT	$DV_{CE0}\frac{P}{V_{bat}} + Dr_{CE}(\frac{P}{V_{bat}})^2 + f_{sw}(E_{on}+E_{off})\frac{DP}{I_{ref}V_{bat}}\left(\frac{V_{ce}}{V_{ref}}\right)^{1.3}$	$2(\lambda_{IGBT} + \lambda_{Diode}) + n_{c2}\lambda_{Cap}$
	Diode	$(1-D)V_{FW0}\frac{P}{V_{bat}} + (1-D)r_F(\frac{P}{V_{bat}})^2 + f_{sw}E_{rr}\left(\frac{(1-D)P}{I_{ref}V_{bat}}\right)^{0.6}\left(\frac{V_{ce}}{V_{ref}}\right)^{0.6}$	
	Capacitor	$\frac{\tan\delta}{2\pi f_{sw}C}(I_h)^2$	

In Table III, m and P are the modulation factor of the dc/ac converter and the input power, respectively. V_{ac} and V_{bat} are the ac-side in the dc/ac converter and the battery-side voltage in dc/dc converter. E_{SW} and f_{SW} are the turn-on and -off energy loss and the switching frequency. V_{ref} and I_{ref} are the voltage and current reference in the datasheet of the IGBT modules. Further, V_{CE0} and r_{CE} are the equivalent voltage and resistance characteristic of the IGBT. V_{FW0} and r_{FW} are the forward voltage and resistance of the diode. E_{rr} is the reverse recovery energy loss of the diode. D is the duty cycle of the dc/dc converter. r_{Lb} as well as I_{Lb} are the resistance and the current of the boost inductor. Moreover, $tan\delta$ is the loss tangent of the capacitor, and I_h is the RMS current of dc-link capacitor. In order to estimate the temperature rise in the components by using the power loss expressions listed in Table III, the thermal model of the components is needed. For the dc/ac and dc/dc converters, the bridge-leg modules connected between the dc terminals, with an upper and a lower IGBT with their anti-parallel diodes and the ac-side connection at the mid-point are considered in this study. The simplified thermal model of such modules is drawn in Fig. 6 [30]. In this model, the thermal resistances are available in the datasheets [31]. To calculate the junction temperature of the semiconductor x, IGBT or forward diode, equation (9) is used.

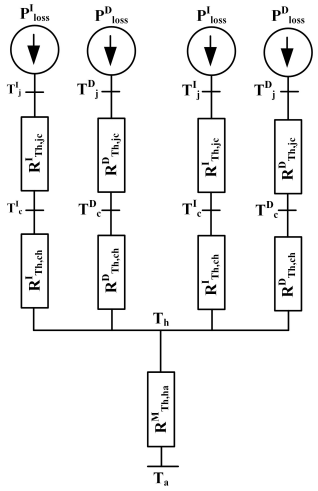

Fig. 6. The simplified thermal model of a double IGBT module.

$$T_j^x = T_a + 2(P_{loss}^D + P_{loss}^I)R_{th-ha} + P_{loss}^x(R_{th-jc}^x + R_{th-jc}^x) \quad (9)$$

C. Sub-system reliability calculation

The S2SC systems are comprised of three sub-systems, GI, OSB and OBB. As it is shown in Fig. 2, the sub-systems are divided into two sections in a double-bus power system. For each bus section of the sub-systems, the block diagrams representation of the sub-systems can be either one of the block diagrams in Fig. 7(a) and (c). For example, the OBB sub-system which consists of a set of N_{OBB} battery packs with their interface converter in parallel can be modeled as the system in Fig. 7(a). Hence, n=N_{OBB} and unit A is equivalent for a pair of a battery pack and a buck/boost converter. The state space of the sub-system can be constructed as the Markov chain drawn in Fig. 7(b), in which i indicates the number of the failed units.

Now, the redundancy is included in the system analysis by defining a redundancy indicator addressing the number of redundant units in the sub-systems. Note that in this paper the redundant units are considered to be active meaning that the units are partially loaded in the nominal operating conditions. Thus, the capacity of the sub-system with m redundant units would not drop below the nominal capacity until the $(m+1)^{th}$ unit failure. Considering $n+m$ units in total, the loading of one healthy unit after failure of i units, $P_{u,i}$ can be calculated by equation (10).

$$P_{u,i} = \begin{cases} \dfrac{P_{total}}{n+m-i} & \dfrac{P_{total}}{n+m-i} < \dfrac{P_{total}}{n} \\ P_r = \dfrac{P_{total}}{n} & o.w. \end{cases} \tag{10}$$

in which P_{total} are the total required power of the sub-system. Then, the capacity of a sub-system after ith failure is equal to $(n+m-i)P_{u,i}$. Thus, by employing the Markov chain analysis in Appendix I, the probabilities of the states are determined. The same analysis can be used for the OSB. The block diagram drawn in Fig. 7(c) can be used to model such sub-systems. In this regard, A-units and B represent active rectifiers and the transformer. The Markov chain of such system is depicted in Fig. 7(d), in which the states with B_i represent the failure of the unit B while there are i A-units failed in the system. The stochastic performance of such system including the probabilities of the states would be obtained by the Markov analysis in Appendix I, and the final failure states which are shown with red line in the Fig. 7(d) would merge into one state by summing their probabilities.

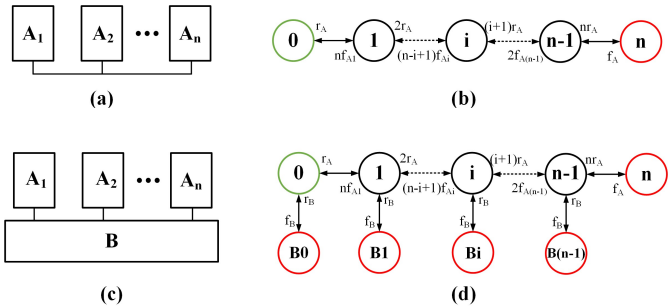

Fig. 7. (a) n-parallel-unit block diagram, (b) n-parallel-unit Markov chain, (c) 1-n-parallel-unit block diagram and (d) 1-n-parallel-unit block diagram (f_{xi} and r_x represent the failure rate at state i and the repair rate of unit x.)

Using the Markov chain analysis for each section of the sub-systems, the probability of the states within a section is obtained in a recursive way, where the increase in the number of A units does not affect the complexity. However, using the Markov chain for the whole sub-system comprising of two (or more in the systems with more busbars) sections would suffer from state-space explosion. Therefore, a UGF method is chosen for this purpose. The UGF u describes the stochastic performance of one sub-system section as following [20].

$$u_{section}(z) = \sum_{i=1}^{n+1} q_i . z^{g_i} \tag{11}$$

In which q_i and g_i accounts for the probability and the capacity of the state i. In order to combine the two UGFs of the sections, a composition operator Ω_1 is defined as following:

$$\begin{aligned} \Omega_1\{u_1, u_2\} &= \Omega_1 \left\{ \sum_{i=1}^{n+1} q_i . z^{g_i} \ , \sum_{i=1}^{n'+1} q'_i . z^{g'_i} \right\} \\ &= \sum_{i=1}^{n+1} \sum_{j=1}^{n'+1} q_i q'_j . z^{(g_i + g'_j)} \end{aligned} \tag{12}$$

Therefore, for a sub-system with two sections the UGF is obtained using (11) and (12).

$$\begin{aligned} u_{sub-sys}(z) &= \Omega_1\{u_{section}, u_{section}\} \\ &= \sum_{i=1}^{n+1} \sum_{j=1}^{n+1} q_i q_j . z^{(g_i + g_j)} \end{aligned} \tag{13}$$

D. S2SC system reliability

In this step all the sub-systems are integrated together to form the stochastic performance of a whole S2SC system. In a S2SC process, the GI and OSB are considered as the sources, so the derated function of them would lead to the decrease in the charging power. Based on the assumption that the battery packs in the OBB do not accept charging power more than their nominal power, and the overcharging is mitigated through control functions, the failure in OBB would decrease the charging power transmitted to the battery packs in total. Since the Markov-based state-space analysis for the whole system suffers from high complexity, the UGF method is employed for the integration of the probabilistic performance of the sub-systems.

For summing the capacity of the GI and OSB, it should be considered that the onshore batteries are recharged through the GI when the vessel is in-route, within t_r. The energy balance of the onshore batteries during one charging break and one trip follows the equality given by

$$(P_{OSB-ch} t_r) - P_{OSB-dis} t_{ch} = (\Delta SoC_{OSB}) C_{OSB}, \tag{14}$$

in which $P_{OSB-ch}, P_{OSB-dis}$ are the charging and discharging power of the onshore batteries. Further, ΔSoC_{OSB} and C_{OSB} are the designed SoC change within one period of operation which is ideally assumed to be zero, and the capacity of the onshore batteries. Thus, the onshore batteries are able to contribute to the charging as far as the GI is able to recharge them within t_r. As a result, it introduces a limit for the capacity of the OSB dependent on the GI capacity.

$$P_{OSB}^{limit} = \frac{(P_{GI} t_r)}{t_{ch}} \tag{15}$$

Therefore, to integrating the GI and OSB, a composition operator Ω_2 is defined as following:

$$\Omega_2\{u_1,u_2\}=\Omega_2\left\{\sum_{i=1}^{n+1}q_i.z^{g_i}\ ,\sum_{i=1}^{n'+1}q_i'.z^{g_i'}\right\}=\sum_{i=1}^{n+1}\sum_{j=1}^{n'+1}q_iq_j'.z^{f\left(g_i.g_j'\right)} \quad (16)$$

$$\text{s.t. f}(P_{GI}.P_{OSB})=\begin{cases}P_{GI}+P_{OSB}^{limit} & P_{OSB}>P_{OSB}^{limit}\\ P_{GI}+P_{OSB} & P_{OSB}\le P_{OSB}^{limit}\end{cases} \quad (17)$$

Then, in order to integrate the probability of the OBB, a composition operator Ω_3 is defined as following:

$$\Omega_3\{u_1,u_2\}=\Omega_2\left\{\sum_{i=1}^{n+1}q_i.z^{g_i}\ ,\sum_{i=1}^{n'+1}q_i'.z^{g_i'}\right\}=\sum_{i=1}^{n+1}\sum_{j=1}^{n'+1}q_iq_j'.z^{(g_i.g_j')} \quad (18)$$

Assuming that all the sub-systems are described by the UGFs, u_{GI}, u_{OSBES}, u_{OBBES} and u_{OR}, by using composition operators (3) and (5), the UGF of the whole system is defined as $u_{S2SCS}(z)$ and calculated as follows:

$$u_{S2SCS}(z)=\Omega_3\{(\Omega_2\{u_{GI}(z),u_{OSB}(z)\}),u_{OBB}(z)\}=\sum_{i=1}^{K}q_i.z^{p_i} \quad (19)$$

In which p_i and q_i are the charging power transmitted and its probability of the state *i*. *K* is also the number of the states. Thus, the probability of charging at least P_{ch} can be calculated as following.

$$Pr(P\ge P_{ch})=\sum_{\{l|p_l\ge P_{ch}\}}q_l \quad (20)$$

IV. Case Study Results and Discussion

In this section, first, the case study is described as a grid-based shore to ship charging system. Then, the reliability of this case study is assessed by the proposed framework and is presented in terms of the defined indicators. To study the effect of OSB, the sizing of the OSB is investigated in the light of the of reliability. The sizing of the OSB with reliability consideration will result in a modified case study. Next, a design routine is carried out for the modified case study, which is one of the main contributions of the proposed framework. In this stage, the modified case study is redesigned thanks to the compatibility of the framework with respect to the system reconfiguration. Here, the size and number of components in the shore-based sub-systems – GI and OSB – are the variables. Based on these variables, design scenarios are introduced. Note that in this design routine it is assumed that the design scenarios are verified thorough the initial design phase which is not the scope of this paper. Further, for the identified best design, the influence of the distributed redundancy is investigated as a practical design factor. Finally, the proposed algorithm is compared with the conventional Markov-chain-based method.

A. Case study description

The case study is inspired by the S2SC system for the all-electric ferry Ellen with 4.3MWh onboard batteries [25]. This ferry is charged by a 4-MW dc S2SC system located in Søby, Denmark. It is worth to mention that the chosen case study is the only S2SC system with the relevant data publicly available for this work, to the best of knowledge of the authors. Here, no onshore batteries are installed to support the distribution grid. Hence, according to the proposed scheme of a S2SC in this paper, this charging system consists of GI and OBB sub-systems. The C-rate of the onboard batteries for charging and discharging are 1 and less than 0.5, respectively. Based on the evaluation report of the E-ferry Ellen, the operational design parameters and the OBB energy profile are listed in Table IV and depicted in Fig. 8, respectively [25]. Note that, the calculated results are highly dependent on the choice of the system configuration and the parts which are chosen by the authors due to the unavailability of the detailed characteristics of the real-case system.

TABLE IV
Operational Parameters of the Case Study

Parameter	Value
Number of trips and charging breaks per day (n)	5/4
Capacity of the onboard batteries	4.3MWh
Nominal S2SC Power	4MW
Average charging time in one day (t_{ch})	25 min
Average sailing time between charging (t_{tr})	2h
Discharged energy from onboard batteries during one trip (E_{tr})	1677kWh
Onboard battery SoC safety range (SoC_{Min} – SoC_{Max})	15%-90%
Nominal onboard batteries SoC range during one trip (SoC_L – SoC_U)	40%-80%

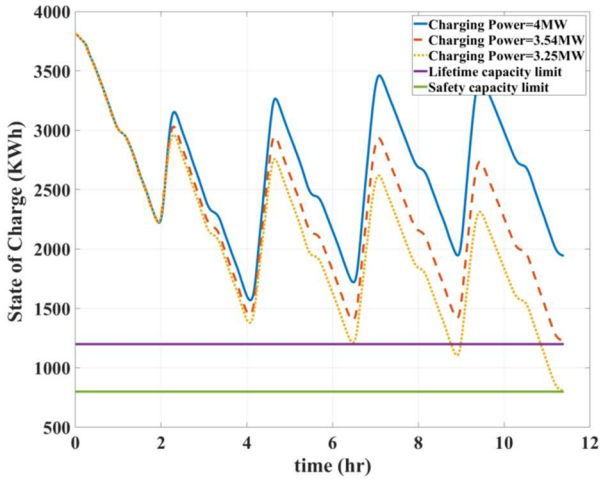

Fig. 8. The OBB energy profile and the required charging power of the case study.

As it can be observed in the OBB energy profile of the case study, two SoC limits are defined as following: 1) lifetime capacity limit, 1200kWh and 2) the safety capacity limit,

800kWh. The blue-colored energy profile is for the nominal charging power of 4MW. According to (1) and (3), two other derated energy profiles are estimated. The dashed, red-colored energy profile represents the marginal energy profile to not violate the lifetime capacity limit. Further, the same procedure has been conducted for the dotted, yellow-colored profile with respect to the emergency limit. In this regard, if the S2SC system capacity has been reduced to a value between the 3.54 and 4MW, the ferry can operate normally. However, if the charging power decreases to below 3.54MW but higher than 3.25MW, the ferry can still operate. In this operation state, although the emergency reserve is kept, the battery lifetime is compromised. Then, for the capacities below the 3.25MW the ferry may not be able to operate anymore since it would not be able to maintain the emergency reserve.

The design parameters of the system aligned with the structure depicted in Fig. 2 is gathered in Table V.

TABLE V
SUB-SYSTEM DESIGN PARAMETERS OF THE CASE STUDY

Sub-units	Parameters	Value
OBB	N_{OBB}	10 per room
	Power rating of battery converters	200kW
	Dc bus voltage	780V
	Battery pack configuration	4s8p42q
	Battery pack nominal voltage and Ah	625V,344Ah
GI	N_{GI}	8 per bus section
	Power rating of grid interface converters	250kW

In the next step, the design parameters of the components are specified in Table VI.

TABLE VI
COMPONENT FAILURE RATES OF THE SYSTEM

Component	Part		Failure rate ($\times 10^{-6}$f/h)
Transformer	winding	Liquid filled Two winding	0.48
Battery Pack	cell	43Ah,3.72V	6.95
dc/ac converter (@fsw=5kHz)	IGBT	FF600R17KE4	13.51
	Diode	FF600R17KE4	
	Capacitor	3×(El-Cap,2kV,0.25mF) +1×(Film-Cap,2kV, 0.01mF)	
dc/dc converter (@fsw=5kHz)	IGBT	FF600R17KE4	16.52
	Diode	FF600R17KE4	
	Capacitor	3×(El-Cap,2kV,0.25mF) +1×(Film-Cap,2kV, 0.01mF)	

Then, the results which are obtained by employing the proposed method for the case study are shown in Table VII.

TABLE VII
AVAILABILITY OF CHARGING POWER IN DIFFERENT OPERATIONAL STATES

Reliability index	Value
LOCE (charging breaks/year)	2.72
DCE (charging breaks/year)	20
Available Power (kW)	3991.55

The results show that the loss of approximately 3 charging breaks is expected within one year of operation and the derated charging breaks in which the charging power is between the charging power threshold and the requested charging power can happen 20 times in the year. However, only for one charging break is it expected that the battery SoC drops below the lifetime limit.

B. The impact of onshore batteries: the system configuration and sizing

Here, the impact on the reliability assessment of the case study by installing onshore batteries is analyzed. First, it is assumed that the onshore battery packs are identical to the onboard battery packs. Therefore, the installed capacity of the GI and OSB are swept by five steps; in this regard, the required number of units are listed in Table VIII. It is obvious that by increasing the installed capacity of OSB the number of the required OSB and GI units increases and decreases, respectively. Then, the reliability framework is carried out for the different arrangements and the results are shown in Fig. 9. It is worth mentioning that the availability of the grid to supply its peak capacity at each design scenario is assumed to be equal to 99.9% [19].

TABLE VIII
THE SUB-SYSTEM UNIT SIZE STEPS

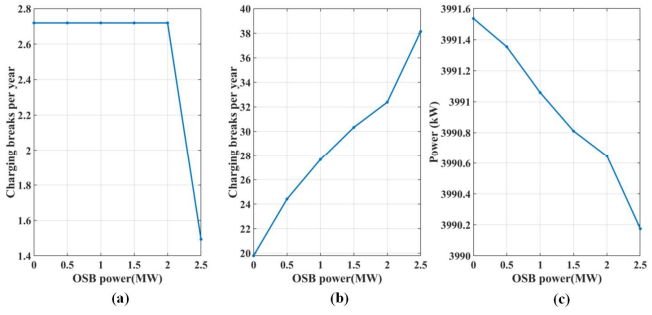

Fig. 9. The impact of using OSB in the S2SC system for the case study on (a) LOCE, (b) DCE and (c) available charging power.

OSB power	0	0.5MW	1MW	1.5MW	2MW	2.5MW
N_{OSB}	0	2	4	6	8	10
Grid Power	4MW	3.5MW	3MW	2.5MW	2MW	1.5MW
N_{GI}	8	7	6	5	4	3

As the results show, the available charging power decreases as the OSB power increases. It is also concluded that the expected number of derated charging breaks increases by 12 breaks per year by adding an OSB sub-system capable of supplying half of the requested charging power. It is because of the high failure rate of the added battery packs. It is obvious from all the figures that stepping from the OSB capacity of 2MW to 2.5MW, the LOCE, DCE and available charging power deteriorates more compared to the other steps. Furthermore, it is not recommended to design the OSB more than 50% because of the additional investment and energy cost as well as the decreased energy efficiency by adding the onshore batteries [4]. Therefore, the installed OSB is chosen to be 2 MWh with 2MW nominal discharging power for the following analysis in this paper.

C. Redesigning of the sub-systems in the case study

Here, the impact of the system configuration within the predefined topology on the reliability of the entire system is studied. To do so, the modified case study is considered with 2MW power from the installed OSB and 2MW power from the GI. In this analysis, the variable parameter is the power rating and the number of the OSB and GI units. For the S2SC system topology defined in this paper, the OSB units consists of a battery pack and its interface dc/dc converter, while the GI units are the dc/ac converters. Note that there is one dedicated transformer for each GI bus section, and it is assumed that the reliability of transformers is not dependent on their size. Considering five various unit ratings for GI and OSB as listed in Table IX and Table X, 25 design scenarios are tested through the reliability framework. Regarding the OSB battery pack configuration, the number of series- and parallel-connected battery cells in the battery modules are changed such that the nominal voltage of the battery packs remain unchanged. To choose the suitable IGBTs and diodes for the units, the voltage and current rating of the devices must be checked, and the thermal design of the device must be considered such that the calculated temperature will be within the allowable junction temperature. To do so, the junction temperature of the IGBTs and diodes are calculated by (9). The thermal resistances are extracted from datasheets [32]. Moreover, the heatsink thermal resistance is assumed to be 0.01k/W with water cooling [30]. Thus, the IGBT and diode with the lowest current rating from Table XIII is selected (considering the condition in (21) is met).

$$T^{x}_{j-calculated} < T^{x}_{jmax-table} \tag{21}$$

TABLE IX
DESIGN STATES FOR SIZING OF OSB FOR THE CASE STUDY

Unit size number	**1**	**2**	**3**	**4**	**5**
OSB unit power rating	$100kW$	200kW	250kW	330kW	500kW
Battery pack Configuration	4s4p42q	4s8p42q	4s10p42q	8s13p42q	8s20p42q
IGBT module number	1	4	5	6	7
N_{OSB}	10	5	4	3	2

TABLE X
DESIGN STATES FOR SIZING OF GI FOR THE CASE STUDY

Unit size number	**1**	**2**	**3**	**4**	**5**
GI unit power rating	$100kW$	200kW	250kW	330kW	500kW
IGBT module number	1	2	4	6	7
N_{OSB}	10	5	4	3	2

By applying the reliability framework on the 25 design scenarios, the results of calculated LOCE and DCE are depicted in Fig. 10. It is obvious from the results shown in Fig. 10 (a) that LOCE is improved by increasing the number of the units. However, the maximum change of LOCE is 0.1 charging break per year. The reason for such negligible change is that the unavailable operation states are caused by at least 6 failed components for the studied design scenarios. As a result, the probabilities of such states are negligible compared to the derated states. It can be seen from the Fig. 10 (b) that the number of derated charging breaks per year decreases as the unit sizes are larger. However, the DCE improvement is more significant as the GI units decreases compared to that for the OSB units because the GI units are made up of three times more semiconductor devices than the OSB units. All in all, if the largest GI and OSB unit sizes are chosen, the DCE is reduced to half compared to the scenario with the smallest GI and OSB units. This observation conveys the fact that adding more components to the system leads into more probable derated operation.

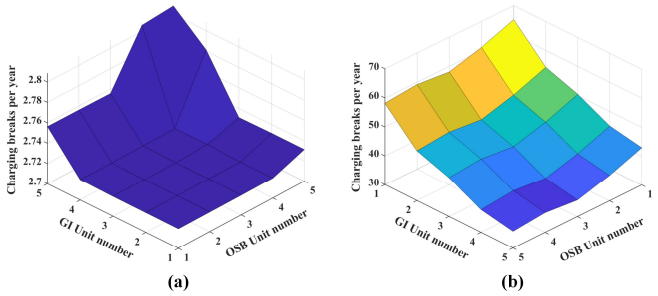

Fig. 10. (a) LOCE and (b) DCE for different GI and OSB unit sizes.

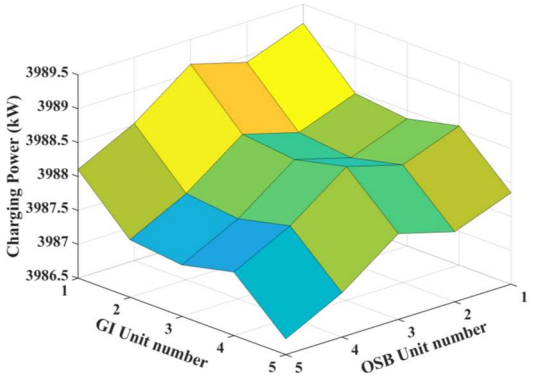

Fig. 11. Available charging power for different GI and OSB unit sizes.

Moreover, the available charging power of the design scenarios can be observed in Fig. 11. The results show that the highest available charging power, which is 3989.25kWh, appears for the design scenario with the smallest unit sizes.

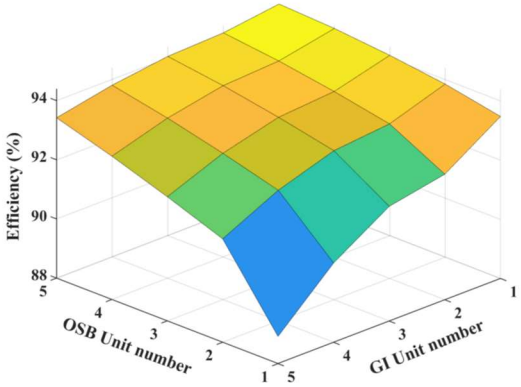

Fig. 12. Calculated energy efficiency for different GI and OSB unit sizes.

In addition to the reliability, the energy efficiency of the charging system has a significant impact on the operation and maintenance expenses of the system. Therefore, to benchmark the design scenarios in a more comprehensive manner, the calculated energy efficiency is considered, besides the reliability. It is calculated by the power loss models in Table III and (8) for the operational profile shown in Fig. 8. To do so, the charging of the onshore batteries by 0.25C-rate in the interval between the two charging breaks is considered. More details about the energy efficiency evaluation for S2SC systems can be found in [4]. Subsequently, the results are shown in Fig. 12.

The energy efficiency results show that the design scenario with 100kW GI unit and the 500kW OSB unit has the highest energy efficiency of 96%. On the other hand, the lowest energy efficiency which is equal to 86% is for the design scenario with the smallest OSB unit and the largest GI unit. It can be concluded that the conduction power loss of the dc/ac converters (relative to I^2) is the dominant term as it grows with the increase of number of the paralleled units. While, for the dc/dc converters, the switching power loss (relative to I) is the dominant power loss because the efficiency drops as the OSB unit power rating decreases.

To take into account both performance indices, the energy efficiency and the reliability, a FoM is defined in (22). Since the objective of the design is to minimize the derated and failed operation and maximize the energy efficiency, the design with the highest FoM can be selected as the design candidate for the system. The results of calculated FoM for 25 design scenarios are depicted in Fig. 13.

$$FoM = \frac{Energy\ Efficiency}{LOCE + DCE} \tag{22}$$

Based on the FoM results, the first three design scenarios with the highest FoMs are suggested as the design candidates and listed in Table XI.

TABLE XI
DESIGN CANDIDATES

Design Candidate	OSB unit	GI unit	LOCE	DCE	Energy Efficiency	FoM
Design #1	$500kW$	$500kW$	2.80	35.83	94.77	0.0241
Design #2	$250kW$	$500kW$	2.75	35.74	94.28	0.0238
Design #3	$333kW$	$500kW$	2.80	36.84	92.39	0.0233

D. Redundancy analysis for the sub-systems of the case study

In the end, the impact of the distributed redundancy on the reliability and the energy efficiency is analyzed. Distributed redundancy refers to the fact that the redundancy in GI and OSB sub-system can have different effects on the whole system. To study the redundancy, in the third step of the reliability framework, as it is described in section III, the capacity levels of the state-space models of the sub-systems are modified by (10). Note that in the previous design stages for the case study, the redundancy was not considered. Here, as an example, the first design candidate, Design #1, is chosen to analyze the redundancy. In this regard, the LOCE+DCE, energy efficiency and FoM are calculated for up to two redundant units in each sub-system bus section. The results are shown in Fig. 14.

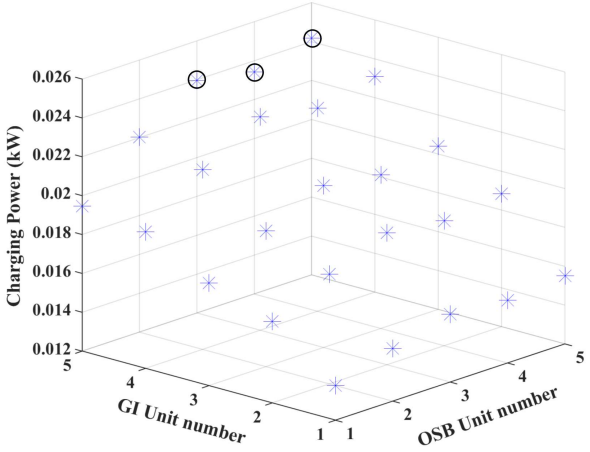

Fig. 13. FoM for the design scenarios.

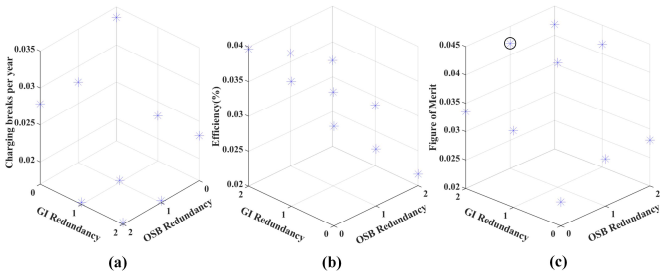

Fig. 14. The impact of the redundancy per section in the sub-systems for the design candidate #1 on (a) LOCE+DCE (b) energy efficiency and (c) Figure of Merit.

As it is shown in Fig. 14(a), the LOCE+DCE decreases to almost half by adding two redundant units in each section of the GI and OSB sub-systems. Additionally, the redundancy in the GI sub-system can have more significant effect on the reduction of unavailability. Based on Fig. 14(b), the efficiency would increase and decrease as the redundancy of the OSB units and GI units increase, respectively. Finally, based on the benchmarking of the redundancy by the FoM in Fig. 14(c), one redundant OSB unit and two redundant GI units can be suggested. However, this would add to the overall cost of the system. For the other design scenarios, the same procedure can be used to investigate the redundancy impact on the reliability and energy efficiency.

E. Comparison with the conventional Markov-chain-based method

To have a better overview of the capability and effectiveness of the proposed algorithm, it is compared with the conventional Markov chain-based method in terms of computation effort, for the same case study. The detailed Markov chain method for the S2SC systems is presented in [16]. For the comparison, the design candidate #1 is considered. Based on the system description in Table V and Table XI as well as the single line diagram in Fig. 2, N_{OBB}, N_{OSB} and N_{GI} are, 10, 2 and 2, respectively. Then, the Markov chain of the whole system includes 9801 operation states. Besides the effort to construct the state-state model in respect to the charging power capacity, the processor must solve 9801 equations to obtain the probability table, and then merge the states to make the equivalent diagram. Conversely, in the proposed framework, in each sub-system, the processor handles only 34 equations thanks to the UGF and modular approach. In the next step, for the same design candidate with two redundant units per each sub-system bus section, as suggested earlier, the number of the operation states escalates to 75625. Furthermore, it is necessary to establish the new state-space manually. On the other hand, employing the proposed framework, assigning the same redundancy adds only 8 more equations to the existing model. Moreover, such procedure is carried out in a recursive algorithm as is described in section III. In the following table, the reliability indices are calculated for the design candidate #1 as an example by the conventional Markov chain and the framework in this paper. It can be seen that the difference between the results from both methods are negligible.

TABLE XII
COMPARISON BETWEEN THE FRAMEWORK AND THE CONVENTIONAL MARKOV CHAIN METHOD

Reliability index	Design candidate #1		Design candidate #1 with two redundancy in GI and OSB	
	Proposed method	*Conventional method*	*Proposed method*	*Conventional method*
LOCE (charging breaks/year)	2.80	2.78	2.71	2.69
DCE (charging breaks/year)	35.83	35.78	19.56	19.55

~~IX.~~ V. CONCLUSION

In this paper, a framework has been developed for the reliability assessment of the S2SC systems, with the main sub-systems such as GI, OSB and OBB. Here, a UGF approach is used for calculating the reliability of the entire system. Power electronics converters, battery packs and transformers are considered as the reliability-critical components of the system. The reliability models of the parts, including semiconductor devices, capacitors and the battery cells are estimated by failure rate models based on historical data. For the power electronics elements, the temperature rise, voltage stress and power loading are also considered in the estimation of the failure rates. Since the S2SC system failure states cannot be described by basic healthy/normal states, a charging power threshold is defined, dividing the operation states into 1) normal, 2) derated and 3) unavailable. For the reliability assessment, three specific indices are introduced such as LOCE, DCE and available charging power. In addition to the reliability indices, the energy efficiency of the design scenarios is considered as an additional factor for selecting the design candidates.

To validate the effectiveness of the proposed method, an extensive case study is conducted on a case inspired by a grid-based dc S2SC system installed and operating in Denmark. Here, the impact of installing onshore batteries and resizing the shore charging sub-systems are analyzed with the defined indices. In the applied design and sizing routine, it is assumed that the design scenarios come from a conventional design phase. Moreover, a FoM is defined with the objective of reducing the unavailability and maximizing the energy efficiency. The results show that the design candidates are the design scenarios with the largest units in the onshore battery and grid interface sub-systems, with respect to the defined FoM. Finally, the distributed redundancy is studied for a selected design candidate. Consequently, in this case, one and two redundant units per section for the onshore battery and grid interface sub-systems is suggested.

Considering the reliability in the design of S2SC systems would help to save costs in terms of unexpected failures and associated maintenance cost during the operation as well as to avoid unnecessary redundancy during the design process. Therefore, the presented design routine can be integrated into the classical design tools. Moreover, the proposed approach can be adopted for other transportation electrification applications, for instance in the charging systems for battery-electric trains, more electric aircrafts, and electric buses. Even though the accuracy of the reliability models is usually compromised for

the sake of simplicity, such models can be widely used to benchmark the preliminary design scenarios. Here, the main point is not the model accuracy but the applicability of the model to compare different design solutions. For this purpose, in addition to the reliability and energy efficiency, the operational and capital expenses of the system can be also considered for the redundancy allocation. For the prospective research, adaptation of the framework to become compatible with studies of the impact from various mission profiles on the reliability of the system is considered.

APPENDIX I

To calculate the probability of the states, the Kolmogorov equation in steady state is used [18]:

$$P \cdot A = 0 \tag{23}$$

where P is the matrix of probability of states and A is the matrix of transition rates in which a_{ij} ($i \neq j$) is the transition rate from state i to state j.

$$P = [P_1\ P_2 \dots P_n] \tag{24}$$

$$A = \begin{bmatrix} a_{11} & \cdots & a_{1n} \\ \vdots & \ddots & \vdots \\ a_{n1} & \cdots & a_{nn} \end{bmatrix} \quad \text{s.t.} \quad a_{ii} = -\sum_{\substack{j=0 \\ j \neq i}}^{n} a_{ij} \tag{25}$$

In order to determine the state probability, only (n-1) row of the equations in (3) with the following equation are considered.

$$\sum_{i=1}^{n} P_i = 1 \tag{26}$$

APPENDIX II

The double IGBT modules from Infineon which are used here are listed in the following table.

TABLE XIII
IGBT MODULES [32]

Module Number	Module
1	FF300R17KE4
2	FF400R17KE4
3	FF500R17KE4
4	FF600R17KE4
5	FF1000R17IE4
6	FF1200R17IP5
7	FF1500R17IP5P

REFERENCES

[1] S. Karimi, M. Zadeh and J. A. Suul, "Shore Charging for Plug-In Battery-Powered Ships: Power System Architecture, infrastructure, and Control," *IEEE Electrification Magazine,* vol. 8, no. 3, pp. 47-61, Sept. 2020.

[2] G. Guidi, J. A. Suul, F. Jenset and I. Sorfonn, "Wireless Charging for Ships: High-Power Inductive Charging for Battery Electric and Plug-In Hybrid Vessels," *IEEE Electrification Magazine,* vol. 5, no. 3, pp. 22-32, 2017.

[3] European Parliament, Council of the European Union, "REGULATION (EU) No 1177/2010 OF THE EUROPEAN PARLIAMENT AND OF THE COUNCIL," *Official Journal of the European Union,* vol. 013, pp. 1-16, 2010.

[4] S. Karimi, M. Zadeh, J. A. Suul, "Evaluation of Energy Transfer Efficiency for Shore-to-Ship Fast Charging Systems," in *2020 IEEE 29th International Symposium on Industrial Electronics (ISIE)*, Delft, Netherlands, 2020.

[5] S. Peyghami, F. Blaabjerg and P. Palensky, "Incorporating Power Electronic Converters Reliability Into Modern Power System Reliability Analysis," *IEEE Journal of Emerging and Selected Topics in Power Electronics,* vol. 9, no. 2, pp. 1668-1681, April 2021.

[6] Q. Xu, Y. Xu, P. Tu, T. Zhao and P. Wang, "Systematic Reliability Modeling and Evaluation for On-Board Power Systems of More Electric Aircrafts," *IEEE Transactions on Power Systems,* vol. 34, no. 4, pp. 3264-3273, 2019.

[7] V. Raveendran, M. Andresen and M. Liserre, "Improving Onboard Converter Reliability for More Electric Aircraft With Lifetime-Based Control," *IEEE Transactions on Industrial Electronics,* vol. 66, no. 7, pp. 5787-5796, July 2019.

[8] B. Stevens, A. Dubey and S. Santoso, "On Improving Reliability of Shipboard Power System," *IEEE Transactions on Power Systems,* vol. 30, no. 4, pp. 1905-1912, July 2015.

[9] M. A. Igder, M. Rafiei, J. Boudjadar and M. -H. Khooban, "Reliability and Safety Improvement of Emission-Free Ships: Systemic Reliability-Centered Maintenance," *IEEE Transactions on Transportation Electrification,* vol. 7, no. 1, pp. 256-266, March 2021.

[10] F. Blaabjerg, H. Wang, I. Vernica, B. Liu and P. Davari, "Reliability of Power Electronic Systems for EV/HEV Applications," *Proceedings of the IEEE,* vol. 109, no. 6, pp. 1060-1076, June 2021.

[11] Y. Yang, A. Sangwongwanich and F. Blaabjerg, "Design for reliability of power electronics for grid-connected photovoltaic systems," *CPSS Transactions on Power Electronics and Applications,* vol. 1, no. 1, pp. 92-103, Dec. 2016.

[12] S. Peyghami, P. Palensky and F. Blaabjerg, "An Overview on the Reliability of Modern Power Electronic Based Power Systems," *IEEE Open Journal of Power Electronics,* vol. 1, pp. 34-50, 2020.

[13] S. V. Dhople, A. Davoudi, A. D. Domínguez-García and P. L. Chapman, "A Unified Approach to Reliability Assessment of Multiphase DC–DC Converters in Photovoltaic Energy Conversion Systems," *IEEE Transactions on Power Electronics,* vol. 27, no. 2, pp. 739-751, Feb. 2012.

[14] J. Guo, X. Wang, J. Liang, H. Pang and J. Gonçalves, "Reliability Modeling and Evaluation of MMCs Under Different Redundancy Schemes," *IEEE Transactions on Power Delivery,* vol. 33, no. 5, pp. 2087-2096, Oct. 2018.

[15] X. Yu and A. M. Khambadkone, "Reliability Analysis and Cost Optimization of Parallel-Inverter System," *IEEE Transactions on Industrial Electronics,* vol. 59, no. 10, pp. 3881-3889, Oct. 2012.

[16] S. Karimi, M. Zadeh and J. A. Suul, "Reliability Analysis of Shore-to-Ship Fast Charging Systems," in *2021 IEEE Transportation Electrification Conference & Expo (ITEC)*, Chicago, US, 2021.

[17] Kanellos, G. J. Tsekouras and F. D., "Ship to shore connection — Reliability analysis of ship power system," in *2016 XXII International Conference on Electrical Machines (ICEM)*, Lausanne, Switzerland, 2016.

[18] M. Rausand , Reliability of Safety-Critical Systems: Theory and Applications, John Wiley & Sons, 2014.

[19] R. N. A. Roy Billinton, Reliability evaluation of power systems, Springer Science & Business Media, 1996.

[20] G. Levitin, The universal generating function in reliability analysis and optimization, London: Springer, 2005.

[21] Z. Liu, C. Tan, and F. Leng, "A reliability-based design concept for lithium-ion battery pack in electric vehicles," *Reliablity Engineering Systems and Safety,* vol. 134, pp. 169-177, Feb. 2015.

[22] M. Liu, W. Li, C. Wang, M. P. Polis, L. Y. Wang and J. Li, "Reliability Evaluation of Large Scale Battery Energy Storage Systems," *IEEE Transactions on Smart Grid,* vol. 8, no. 6, pp. 2733-2743, Nov. 2017.

[23] E. Chatzinikolaou and D. J. Rogers, "A Comparison of Grid-Connected Battery Energy Storage System Designs," *IEEE Transactions on Power Electronics,* vol. 32, no. 9, pp. 6913-6923, Sept. 2017.

[24] G. Sulligoi, A. Vicenzutti and R. Menis, "All-Electric Ship Design: From Electrical Propulsion to Integrated Electrical and Electronic Power Systems," *IEEE Transactions on Transportation Electrification,* vol. 2, no. 4, pp. 507-521, Dec. 2016.

[25] A. Kortsari, L. Mitropoulos, T. Heinemann and H. H. Mikkelsen, "Prototype and full-scale demonstration of next-generation 100% electrically powered ferry for passengers and vehicles: Evaluation report of the E-ferry," 2020.

[26] A. Aa, "Brodrene Aa and The Fjords pioneering with "Future of The Fjords" – offering zero emisson fjord cruise," [Online]. Available: https://static1.squarespace.com/static/5b18ec3cee1759b32d884907/t/5ca7401a419202c6a737dac1/1554464803172/2019+04+Article+Future+of+The+Fjords.pdf. [Accessed 10 12 2019].

[27] Military Handbook: Reliability Prediction of Electronic Equipment: MIL-HDBK-217F, US: Department of defense, Dec. 1991.

[28] "INTERNATIONAL ATOMIC ENERGY AGENCY, Generic Component Reliability Data for Research Reactor PSA," IAEA-TECDOC-930, Vienna, 1997.

[29] P. Tu, S. Yang and P. Wang,, "Reliability- and Cost-Based Redundancy Design for Modular Multilevel Converter," *IEEE Transactions on Industrial Electronics,* vol. 66, no. 3, pp. 2333-2342, March 2019.

[30] R. Schnell, M. Bayer and S. Geissmann, "Application Note 5SYA 2093-00: Thermal design and temperature ratings of IGBT modules," ABB, Lenzburg, Switzerland, 2013.

[31] "AN2015-10: Transient thermal measurements and thermal equivalent circuit models," infineon, Munich, Germany, 2020.

[32] "IGBT Modules," Infineon, [Online]. Available: https://www.infineon.com/cms/en/product/power/igbt/igbt-modules/. [Accessed 25 March 2021].

Siamak Karimi (SM'20) was born in Shiraz, Iran, in 1994. He received his B.Sc. degree in electrical engineering from University of Tehran, Tehran, Iran in 2016, and his M.Sc. in power electronics from Sharif University of Technology, Tehran, Iran in 2019. He is currently working towards his Ph.D. in the department of marine technology at the Norwegian University of Science and Technology (NTNU), Trondheim, Norway. His research interest are design, modeling and control of onboard power system and battery charging infrastructure for electrified transportation, especially ships.

Mehdi Zadeh (M'11) received the Ph.D. degree in Electrical Engineering from Norwegian University of Science and Technology (NTNU), Trondheim, Norway, in 2016. From 2016 to 2017, he was with the power electronics industry, working on the development of battery charging systems. In 2017, he joined the Marine Technology Centre at NTNU in Trondheim, where he is currently an Associate Professor of Hybrid Power Systems and the director of the Marine Electrification Research Lab. His main research interests include onboard power electronics, marine electrification, low-emission and autonomous shipping, and offshore renewable energy systems.

Jon Are Suul (M'11) received the M.Sc. degree in energy and environmental engineering and the Ph.D. degree in electric power engineering from the Norwegian University of Science and Technology (NTNU), Trondheim, Norway, in 2006 and 2012, respectively.

From 2006 to 2007, he was with SINTEF Energy Research, Trondheim, where he was working with simulation of power electronic converters and marine propulsion systems until starting his Ph.D. studies. Since 2012, he has been a Research Scientist with SINTEF Energy Research, first in a part-time position while working as a part-time Postdoctoral Researcher with the Department of Electric Power Engineering of NTNU until 2016. Since August 2017, he has been an Adjunct Associate Professor with the Department of Engineering Cybernetics, NTNU. His research interests are mainly related to modelling, analysis, and control of power electronic converters in power systems, renewable energy applications, and electrification of transport.